inorganics

MDPI

Article

Synthesis and Characterization of Broccoli-like Ag/Cu_2O Nanostructures on ZnO Nanowires Using the Plasma–Liquid Interaction Method

Phung Thi Thu [1], Ta Ngoc Bach [2], Le Thi Hong Phong [2], Do Hoang Tung [3], Vu Hong Ky [2], Do Khanh Tung [2], Vu Dinh Lam [4], Do Hung Manh [2], Nguyen Huy Dan [2], Trinh Xuan Anh [5] and Ngo Thi Hong Le [2,4,*]

[1] University of Science and Technology of Hanoi, Vietnam Academy of Science and Technology, 18 Hoang Quoc Viet, Cau Giay, Hanoi 100000, Vietnam; thuphungi2@gmail.com
[2] Institute of Materials Science, Vietnam Academy of Science and Technology, 18 Hoang Quoc Viet, Cau Giay, Hanoi 100000, Vietnam; bachtn.ims@gmail.com (T.N.B.); lephong.ims@gmail.com (L.T.H.P.); kyvuhong@gmail.com (V.H.K.); dokhanhtung@gmail.com (D.K.T.); manhdh@ims.vast.ac.vn (D.H.M.); dannh@ims.vast.ac.vn (N.H.D.)
[3] Institute of Physics, Vietnam Academy of Science and Technology, 18 Hoang Quoc Viet, Cau Giay, Hanoi 100000, Vietnam; dhtung@gmail.com
[4] Graduate University of Science and Technology, Vietnam Academy of Science and Technology, 18 Hoang Quoc Viet, Cau Giay, Hanoi 100000, Vietnam; lamvd@gust-edu.vast.vn
[5] Department of Chemistry, School of Chemistry and Life Sciences, Hanoi University of Science and Technology, 1 Dai Co Viet, Hanoi 100000, Vietnam; trinhxuananh@gmail.com
* Correspondence: hongle@ims.vast.ac.vn or hongle2009@gmail.com

Abstract: We have designed an excellent visible-light-driven and high-performance photocatalyst with a Ag-Cu_2O-ZnO nanowire heterostructure in our work by combining the hydrothermal approach with plasma–liquid technology. The structural and morphological characteristics and optical properties of the samples were evaluated using X-ray diffraction, field-emission scanning electron microscopy, and spectrophotometry, respectively. The results show that the Ag nanoparticles are mainly positioned on the Cu_2O nanoclusters compared with the ZnO nanowire surface, forming broccoli-like Ag-Cu_2O nanoclusters during the Ar gas plasma treatment process in an aqueous solution. The diameter of the Ag/Cu_2O nanoclusters ranges from 150 to 180 nm. The Ag-Cu_2O-ZnO nanowires exhibited improved photocatalytic performance, decomposing approximately 98% methyl orange dye in 30 min. This is a consequence of the synergistic interactions between the p-n heterojunction formed at the Cu_2O-ZnO interfaces and the localized surface plasmon resonance (LSPR) effect of the Ag nanoparticles, which broaden the visible light absorption range and effectively separate the photogenerated charge carriers.

Keywords: ZnO nanowires; plasma–liquid; photocatalysis; methyl orange; localized surface plasmon resonance; hydrothermal method

Citation: Thu, P.T.; Bach, T.N.; Phong, L.T.H.; Tung, D.H.; Ky, V.H.; Tung, D.K.; Lam, V.D.; Manh, D.H.; Dan, N.H.; Anh, T.X.; et al. Synthesis and Characterization of Broccoli-like Ag/Cu_2O Nanostructures on ZnO Nanowires Using the Plasma–Liquid Interaction Method. *Inorganics* **2024**, *12*, 80. https://doi.org/10.3390/inorganics12030080

Academic Editors: Sake Wang, Minglei Sun and Nguyen Tuan Hung

Received: 31 December 2023
Revised: 27 February 2024
Accepted: 29 February 2024
Published: 6 March 2024

1. Introduction

In recent decades, the photocatalytic approach has demonstrated exceptional benefits for both environmental protection and the rehabilitation of polluted water [1]. Breakthrough achievements in nanomaterial synthesis technology have contributed to accelerating the catalytic process to satisfy practical needs. Semiconductors have drawn a lot of interest as a key contender among the representative catalysts [1,2]. However, a challenging problem nowadays is the quick recombination rate of the electron–hole pairs produced in photocatalytic reactions [1,2]. It is imperative to address this bottleneck to produce a high-performance photocatalyst.

In parallel with the well-known typical semiconductors, thanks to their high catalytic activity, affordable cost, nontoxicity, and facile preparation, both ZnO and copper(I) oxide

(Cu_2O) have emerged as prominent candidates [3–6]. Typically, ZnO nanowires have a highly promising shape among ZnO 1D structures because of effective electron transport in narrow dimensions and their anisotropy [3,7]. Nevertheless, ZnO nanowires only absorb 3–5% of visible light because they have a large band gap (>3 eV) [7]. Therefore, the exploitation of a ZnO/Cu_2O heterojunction is expected to slow down the charge carrier recombination rate—since there exists an irreversible electric field at the p-n junction of the ZnO/Cu_2O system—and expand the absorption spectrum toward the visible light range, as shown in previous articles [8–11]. Furthermore, the concordance between the energy level and the electronic structure in the ZnO and Cu_2O forms a superior catalytic p-n system compared with other p-n systems [8–13]. On the other hand, the formation of a Schottky barrier at the precious metal–semiconductor interface can efficiently prevent the recombination of electron–hole pairs [14–16]. Combined with the surface plasmonic resonance effect of noble metal nanoparticles, which provides a considerable adsorption ability in the visible light region, precious metal/semiconductor-based catalysts greatly increase the photo-decomposing process [14–19]. In addition to mono- and binary structures, ternary structures have been recently developed and offer highly promising potential. The synergistic effects between the interfaces in ternary structures bring out the possibility of boosting the charge carrier separation and triggering the absorption range in the visible light region [20–28]. The ZnO/Au/Cu_2O heterojunction system, as described by Yuan et al., demonstrates a better Z-scheme charge separation and deep oxidative decomposition for organic dye, resulting in enhanced catalytic performance of over 78% compared with pure ZnO [27]. Tsai et al. showed that Ag/Cu_2O/ZnO NRs with remarkable kinetic constant enhancements degrade RhB more effectively than Ag/ZnO and Cu_2O/ZnO [23]. Numerous well-known fabrication methods for ZnO nanowires have been applied, such as carbo-thermal evaporation [29], metal–organic vapor phase epitaxy [30], and molecular beam epitaxy [31]. Unfortunately, these methods have disadvantages, such as being time-consuming, costly, and complicated experimental systems. Studies have demonstrated that the fabrication of ZnO nanowires using the hydrothermal method is simple and economical. Additionally, various fabrication techniques for mono- and binary structures, as well as ternary structures—including co-precipitation [32], hydrothermal [27], sol–gel [14], solution combustion [33], and plasma technology [28,34,35]—have been applied. Moreover, plasma technology has increasingly satisfied the urgent requirement for the development of a quick, easy, and eco-friendly approach. The interaction between plasma and aqueous solutions at the interface has been found to offer a strong solution for the synthesis and functionalization of nanomaterials [36,37]. In this case, the plasma is generated either inside the solution or close to its surface. Importantly, more active species, such as electrons, radicals, ions, and produced UV light, are introduced to promote reactions in the solution [36,37]. To the best of our knowledge, the use of the plasma–liquid approach to construct ternary heterostructures and simultaneously study their underlying formation mechanisms is still limited.

Therefore, we recently synthesized a CuO-Ag-ZnO nanowire photocatalyst in which Ag nanoparticles were intercalated between the CuO nanoparticles and the ZnO nanowire using the plasma–liquid method in alkaline media [28]. However, that work did not mention the formation mechanism of the nanoparticles on the ZnO nanowires during the plasma treatment. Additionally, to understand the comprehensive scenario of the influence of the media on the formation of nanoparticles on ZnO nanowires under plasma conditions and to study the effect of the composite order, from semiconductor–metal–semiconductor to metal–semiconductor–semiconductor, on photocatalytic activity, we designed and prepared a ternary heterostructure made of Ag-Cu_2O-ZnO nanowire in this work. In acidic media, Cu_2O particles were formed instead of CuO particles under the same plasma conditions. Furthermore, the Ag nanoparticles were preferentially located in Cu_2O nanoclusters instead of the ZnO nanowires, forming a broccoli-shaped structure attached to the ZnO nanowires. The results showed that the presence of Ag and Cu_2O partially quenched the photoluminescence in both the UV and visible light regions. Consequently,

the photocatalytic activity decomposing methyl orange in the ternary Ag-Cu_2O-ZnO structure took place strongly within 30 min with an efficiency of approximately 98%. The stability and photo-reusability were dramatically improved, merely decreasing by about 3% in terms of performance after 20 cycles. The formation of the Ag-Cu_2O-ZnO heterostructure within the plasma–liquid treatment is also discussed in detail.

2. Results and Discussion

2.1. Decorating Ag NPs and Cu_2O NPs on ZnO NWs via the Plasma–Liquid Interaction Method

ZnO nanowires (NWs) were prepared using the hydrothermal method [28]. The ZnO-nanowire-growing procedure involves a mixed aqueous solution as a precursor, which contains the alkaline reagent Na_2CO_3 and Zn^{2+} salt. The formation process of the ZnO was provided by Hu et.al. [38].

The interaction between the Ar gas plasma and the aqueous solution can generate strongly reactive species such as atomic hydrogen (H), H*, H^+, and OH radicals, caused by the dissociation of water molecules (H_2O), hydrated electrons (e^-_{aq}), and UV light—which has a strong reducing ability—at the same time [39–42]. These species take part in and push up the reactions in the solution. The decoration of the Ag and Cu_2O NPs on the ZnO NWs using the plasma–liquid treatment includes the following stages: Firstly, the H^+ species participate in the bombarding process on the surface of the ZnO NW, resulting in the removal of oxygen atoms and, thus, the creation of oxygen vacancies on the surface. Consequently, the nanoparticle adherence to the ZnO surface is greatly enhanced. This process was considered for a Pt-attached MoO_x system [41] by the Li group and activated TiO_2 [39] by the Yu group. Secondly, the reduction reaction of metal ions, in order to synthesize nanoparticles in the plasma–liquid process with the reducing agents e^-_{aq} and H*, is performed as per the following equations [37,43]:

$$Ag^+ + ne^-{}_{aq} \rightarrow Ag^0 \quad (1)$$

$$Ag^+ + H^* \rightarrow Ag^0 + H^+ \quad (2)$$

The hydroxyl OH radicals produced at the plasma–liquid interface location react swiftly with Cu^{2+} together with ascorbic acid in order to form Cu_2O nanoparticles, as per the reaction below [44]:

$$Cu^{2+} + OH^- + C_6H_8O_6 \rightarrow Cu_2O + C_6H_6O_6 + H_2O \quad (3)$$

Lastly, the ZnO nanowires can make electron–hole pairs on their surface by absorbing the UV light generated within the plasma process. On the ZnO surface, these electrons and holes are utilized for direct reduction or to produce radicals that further reduce Ag^+ and Cu^{2+} ions [34,45]. Notably, Ag and Cu_2O nanoparticles preferentially agglomerate with each other to form a broccoli-like hierarchical structure because of their energy priority [46]. With the benefits of being rapid and easy to use, the plasma–liquid method can effectively produce a Ag-Cu_2O-ZnO ternary structure without adding chemical surfactants as other methods require.

2.2. Structural and Morphological Characteristics

Figure 1 introduces the XRD patterns of as-prepared samples: ZnO and Ag-Cu_2O-ZnO NWs determined by a Bruker D8 advanced X-ray power diffractometer device. The diffraction peaks characterize the hexagonal wurtzite structure of the ZnO NWs located at 31.9°, 34.5°, 36.4°, 47.66°, 56.69°, and 63.1° corresponding to crystal planes of (100), (002), (101), (102), (110), and (103), in excellent consistency with the standard card of ZnO (JCPDS: 36-1451). Remarkably, these peaks are all shown in Ag-Cu_2O-ZnO X-ray diffraction patterns without any shifting, indicating the advantage of the plasma–liquid method, which does not destroy the ZnO crystalline structure. The presence of diffraction peaks with Miller indices (011), (002), and (022), matching the standard card of Cu_2O (JCPDS: 05-0667),

confirms the presence of Cu_2O, as pointed out in other published articles [9,11,44]. A peak at around 43° can be due to the overlap contribution of the Ag (200) and Cu_2O (002) planes. A peak at around 38° can be attributed to the (111) plane of Ag nanoparticles, corresponding to the standard card of Ag (JCPDS: 04–0783). From the X-ray diffraction pattern, a ternary Ag-Cu_2O-ZnO composite was successfully synthesized using the plasma–liquid method. Furthermore, no other X-ray peaks could be observed, confirming the purity of the as-prepared samples.

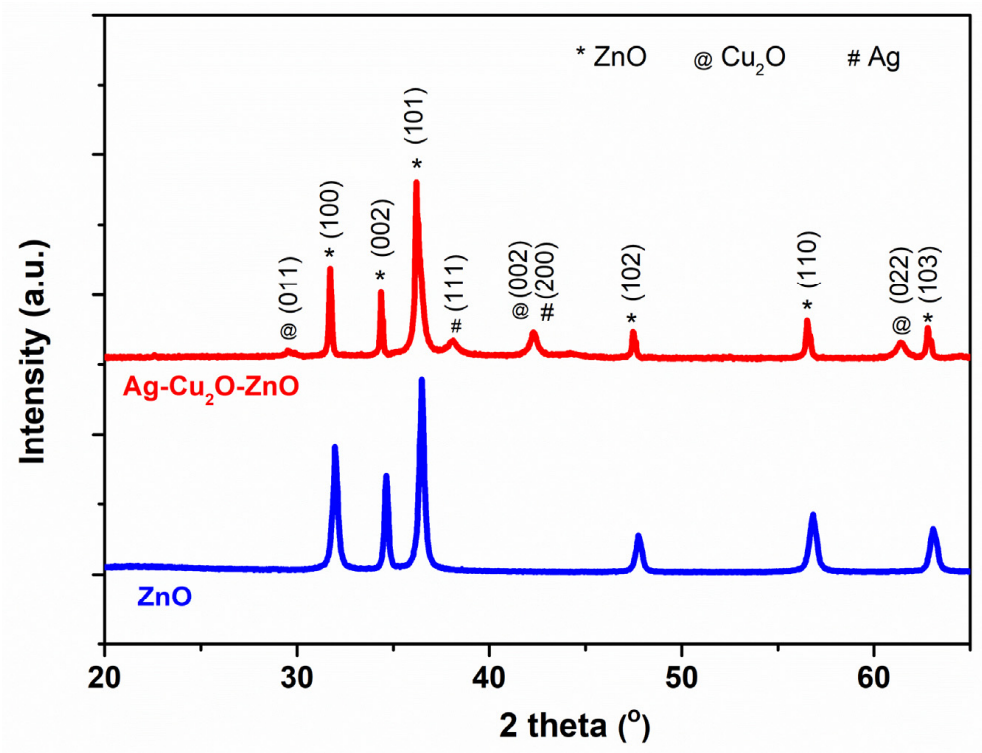

Figure 1. XRD patterns of ZnO and Ag-Cu_2O-ZnO synthesized using the hydrothermal approach combined with the plasma–liquid method.

The surface morphologies of ZnO and Ag-Cu_2O-ZnO NWs measured by FESEM are displayed in Figure 2. The ZnO NWs prepared using the hydrothermal technique have diameters of 20–70 nm and lengths of approximately 10 µm (Figure 2a,b). Under the impact of plasma current, the Cu_2O and Ag nanoparticles were decorated on the surfaces of the ZnO NWs (Figure 2c) in a broccoli-like shape. As a result, broccolis with 150–180 nm diameters are observed. The particle size distribution histogram of the Ag NPs and Cu_2O NPs is shown in Figure 2d. The average particle size of the nanoparticles was calculated to be 10.3 nm from the original data. The broccoli shape is an overlay result of the consecutive formation of Cu_2O crystals together with the deposition of Ag nanoparticles. To elucidate this, we implemented EDX-STEM mapping to measure the Ag-Cu_2O-ZnO composite (Figure 2e). Obviously, four elements—Zn (blue), Cu (red), Ag (green), and O (yellow)—were detected, and one cannot observe any other elements. It is worth mentioning that the majority of Ag elements are located in the broccoli of Cu_2O NPs. HRTEM images robustly demonstrated the existence of distinguishable lattice fringes of ZnO, Cu_2O, and Ag with d-spacings of 0.25 nm, 0.24 nm, and 0.23 nm, respectively, which are assigned to crystal planes of (101) (ZnO), (111) (Cu_2O), and (111) (Ag), as shown in Figure 3. Thus, both Ag and Cu_2O NPs were successfully decorated on the ZnO NW surfaces.

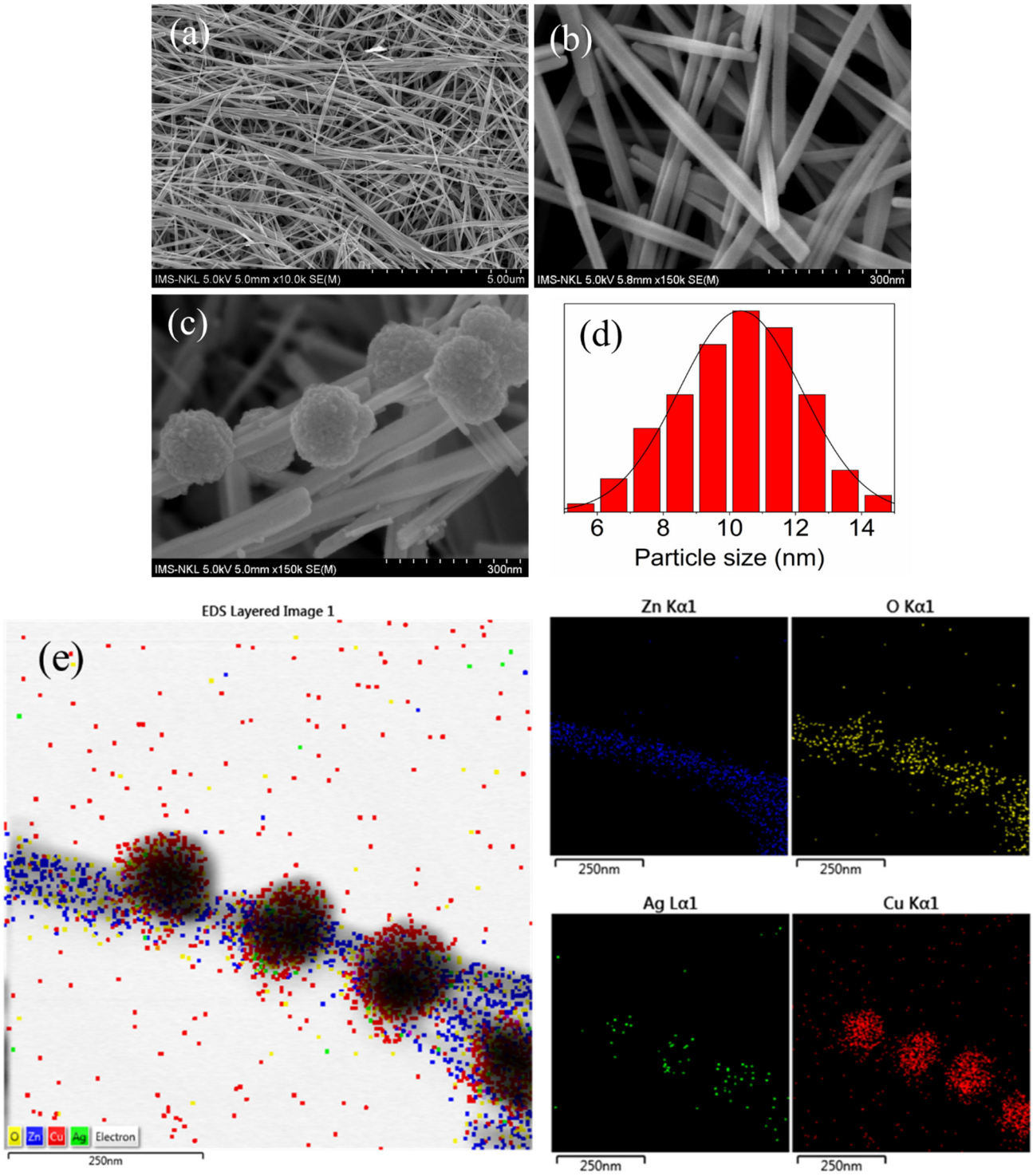

Figure 2. Field-emission scanning electron microscopy images of ZnO (**a**,**b**) and Ag-Cu_2O-ZnO NWs (**c**); particle size distribution histogram of Ag NPs and Cu_2O NPs (**d**); and EDX-STEM mapping images of Zn, O, Ag, and Cu elements (**e**).

Analysis of the room-temperature PL spectra of the ZnO and Ag-Cu_2O-ZnO NWs showed that the spectrum intensity gradually declined at both the UV and VIS regions when the Cu_2O and Ag NPs were attached (Figure 4a). As reported in previous articles [28,46], the PL spectrum of ZnO NWs consists of an emission peak in the 380–390 nm region, which stems from free electron–hole pair recombination, and a broad emission peak in the visible region, which arises from defect levels [46]. Therefore, the suppression of the PL spectrum

of ZnO NWs is a crucial task in gaining an excellent photocatalyst. As expected, a part of the PL spectrum is quenched upon the decoration of Cu_2O and Ag NPs on the ZnO NWs surface, indicating an inhibition in electron–hole pair recombination and an increase in charge separation efficiency [47]. The reason for the decrease in the PL spectrum intensity can be ascribed to (1) the heterostructure formation between the ZnO and Cu_2O, improving the charge transfer route, and (2) the formation of an 'electron reservoir' by the Ag NPs to catch the photogenerated electrons.

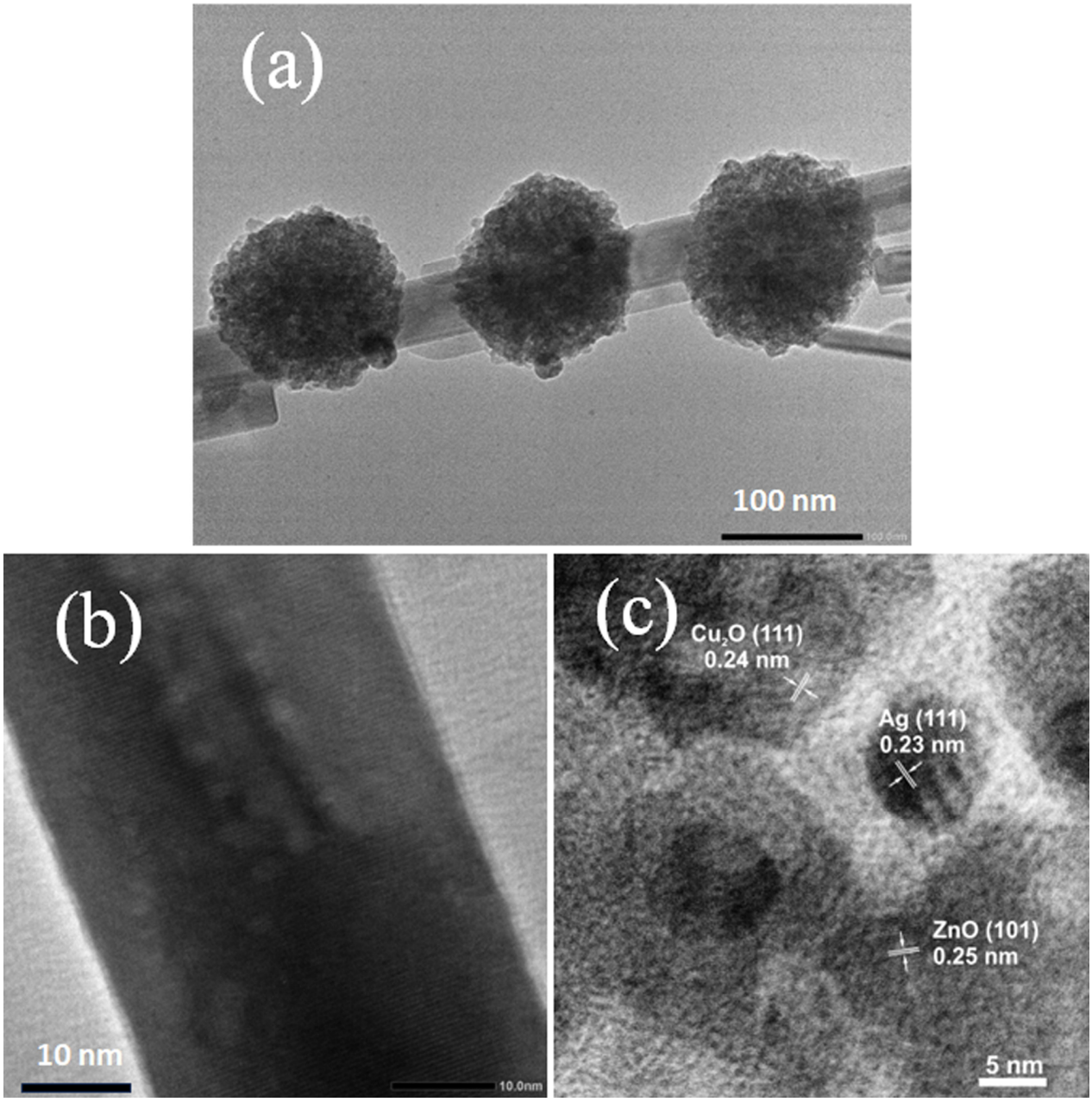

Figure 3. TEM (**a**) and HR-TEM images of ZnO NW (**b**) and Ag-Cu_2O-ZnO (**c**).

The optical absorption spectra of ZnO and Ag-Cu_2O-ZnO samples are studied and depicted in Figure 4b. Obviously, the ZnO NWs only absorb in the UV region with an absorption edge at ~385 nm. In the ternary Ag-Cu_2O-ZnO NWs, the absorption edge moves forward along the wavelength side, and a broad absorption range is found in the visible light region. This is a consequence of the narrower bandgap of Cu_2O [48] and the localized surface plasmon resonance (LSPR) effect of Ag NPs, which forms an LSPR

peak at ~445 nm. Therefore, the enhanced absorbance in the visible light region produces more photogenerated charge carriers. These findings also confirm the formation of a Ag-Cu_2O-ZnO heterojunction.

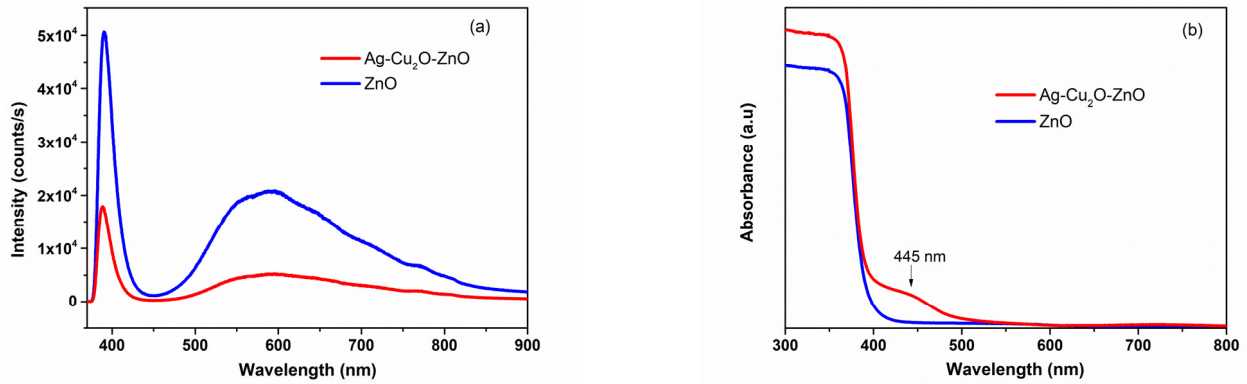

Figure 4. PL spectra (**a**) and absorbance spectra (**b**) of ZnO and Ag-Cu_2O-ZnO.

2.3. Photocatalytic Activity

Electrochemical impedance spectroscopy (EIS) is exploited as a useful tool for learning more information about charge separation/transfer and charge recombination in photocatalysts. Interface layer resistance on the electrode surface is exhibited by an arc radius on a Nyquist plot. As shown in Figure 5a, the arc radius for the Ag-Cu_2O-ZnO NWs is significantly smaller than that of their pure ZnO counterpart, indicating that this ternary heterostructure possesses faster interfacial charge transfer and more efficient charge separation. On the other hand, as noted in numerous articles, the higher photocurrent demonstrates the better separation efficiency of the charge carriers. Therefore, the photocurrent versus the time of the as-prepared samples was measured in three on–off irradiation cycles using solar-simulated light and then plotted in the inset of Figure 5a. It is evident that the photocurrent intensity is greatly enhanced when the Ag and Cu_2O NPs are decorated on the ZnO NW surface. As a result, the current intensity of the Ag-Cu_2O-ZnO NWs is about 600×10^{-9} A/cm^2, three times higher than that of pure ZnO NWs. Consequently, the Ag-Cu_2O-ZnO NWs unquestionably exhibit a more effective photogenerated electron–hole separation ability. Furthermore, the interfacial electric field forming in the Ag-Cu_2O-ZnO may also be responsible for these observations since they hasten the migration of charge carriers under UV–vis light.

The degradation of methyl orange (MO) dye with respect to time under solar simulator illumination is used to estimate the photocatalytic activity of the ZnO and Ag-Cu_2O-ZnO samples. The decrease in MO absorption peak intensity between 350 and 550 nm is considered a crucial indicator for this study. Figure 5b,c show the UV–vis absorption spectra of the MO dye in terms of irradiation time using the ZnO and Ag-Cu_2O-ZnO photocatalysts, respectively. As indicated, the MO dye is decolorized based on illumination time. A peak shift to a shorter wavelength side can also be found, which is explained by the formation of intermediate species during photocatalytic reaction [33,49].

As seen in Figure 5b,c, the MO dye was strongly decomposed, ~27% and 82% in the first 10 min and ~89% and 98% within 30 min, corresponding to pure ZnO and Ag-Cu_2O-ZnO NWs. This is assumed to be due to the mutual working of the active species—•OH, $\bullet O_2^-$ photogenerated holes, and electrons—in decomposing organic molecules in the aqueous solution. Since •OH and $\bullet O_2^-$ are generated by surface redox during photocatalysis, photogenerated holes and electrons can have a key impact on the degradation of organic dyes.

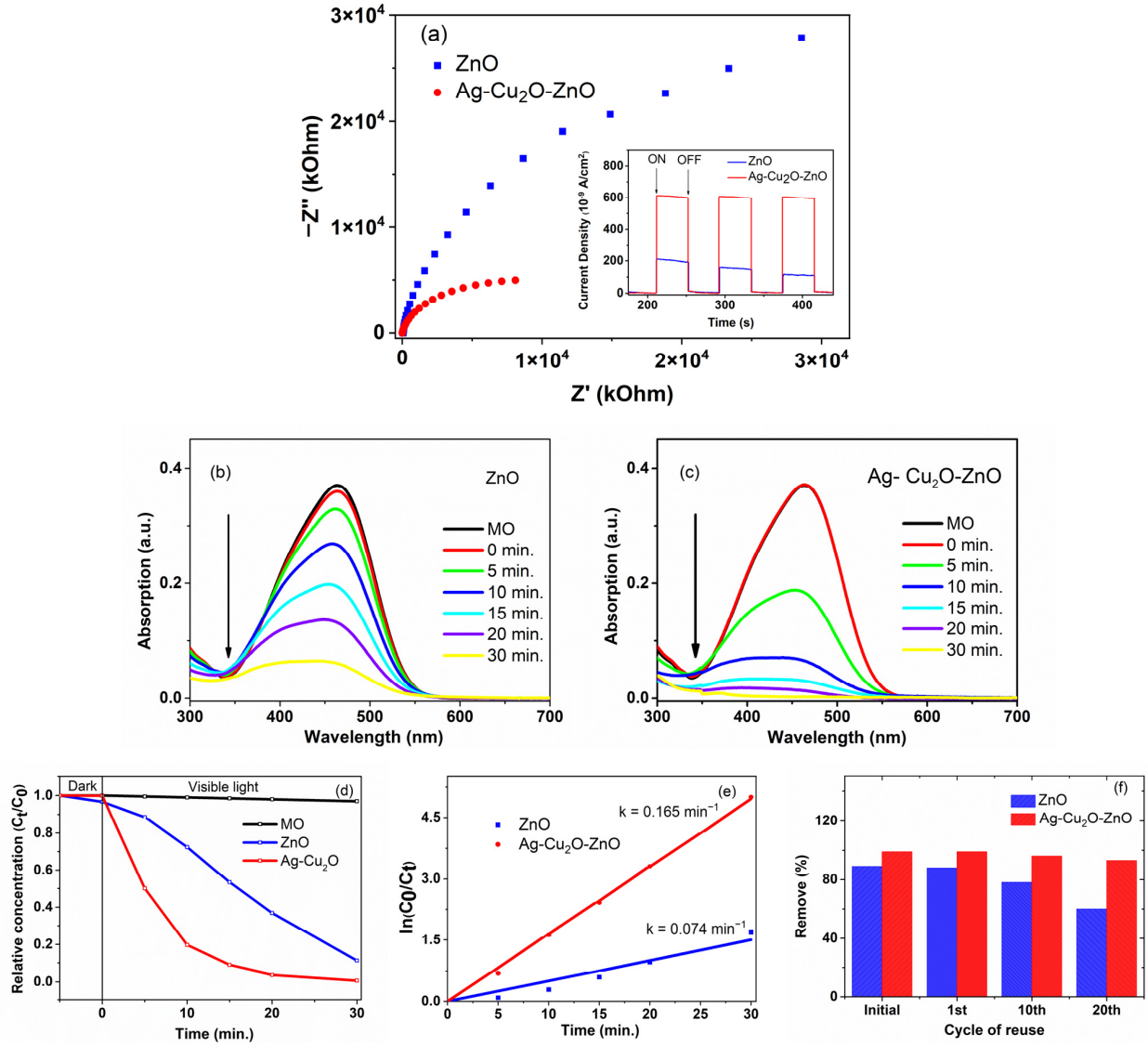

Figure 5. EIS Nyquist plot curves of ZnO and Ag-Cu_2O-ZnO samples. The inset is the photocurrent-time curves of as-prepared samples under on–off solar-simulated light (**a**). The UV–vis absorption spectra of the MO dye in terms of time under solar-simulated light using the photocatalysts of ZnO (**b**) and Ag-Cu_2O-ZnO (**c**). C_t/C_0 curves as a function of the time of the MO degradation process (**d**). Kinetics of the MO degradation process (**e**). Photocatalytic activity reuse cycle of Ag-Cu_2O-ZnO NWs compared with ZnO NWs (**f**).

For further information, the kinetics (k) of the MO decomposing reaction was calculated with the Langmuir–Hinshelwood equation [28]. The k-values of the ZnO and the Ag-Cu_2O-ZnO NWs were 0.074 min^{-1} and 0.165 min^{-1}, respectively. Evidently, these findings indicate that the Ag/Cu_2O broccolis contribute to accelerating the MO photo-decomposing process of ZnO host material more quickly. Therefore, the necessary decomposing time is much shorter in comparison with pure ZnO NWs.

It is worth mentioning that the k-value of the Ag-Cu_2O-ZnO NWs is greater than the compounds used in many previous papers, as seen in Table 1. The k-values of the binary composites, TiO_2-ZnO (0.011 min^{-1}) and ZnO-WO_3 (0.0521 min^{-1}), are ~15 and 3 times lower than that of Ag-Cu_2O-ZnO, respectively. In the Ag-Cu_2O-ZnO nanorods prepared by Tsai et al. [23], their degradation rate was only 0.041 min^{-1}, equal to ¼k of our composite. Another composite, ZnO-Au-Cu_2O nanorods [24], showed excellent photocatalytic performance driven by visible light; nevertheless, the k-value (0.3495 h^{-1})

was a limitation of this structure. Similarly, WO_3-ZnO@rGO, ZnO-CdO-CuO, and ZnO-Fe_3O_4-g-C_3N_4 composites have ~6–7 times lower k-values compared with our Ag-Cu_2O-ZnO NWs. Consequently, these composites took much more time to photodegrade organic dyes. It can be confirmed that decorating Ag-Cu_2O NPs on ZnO wires is a superior strategy. This finding has also been found in a CuO-Ag-ZnO nanowire structure in our previous report [28]. In that work, the MO dye is completely decomposed in 30 min at a high k-value of 0.2007 min^{-1}. This k-value difference may originate from the main interfaces between the CuO-Ag-ZnO and Ag-Cu_2O-ZnO structures. In the CuO-Ag-ZnO NWs, the formation of the interfacial electric field in the semiconductor–metal–semiconductor was demonstrated to further improve photocatalytic efficiency [28]. The electrons in the CuO NPs excited from the valance band to the conduction band can transfer to the Fermi level of the Ag NPs and the ZnO conduction band. Then, the electrons from the Fermi level can also move into the conduction band of the ZnO; thus, more electrons participate in the photocatalytic process.

Table 1. A comparison of the photocatalytic performance of different systems.

Structure	Method	Organic Dye	Kinetics k	Yield (%)	Time (min)/Ref.
Cu_2O-ZnO/kaolinite	Co-precipitation	MB	0.098 min^{-1}	93	105 [32]
Cu_2O-ZnO	Precipitation and calcination	MO	1.30762 h^{-1}	98	240 [13]
Ag-Cu_2O-ZnO	Hydrothermal and photoreduction	RhB	0.041 min^{-1}	80	60 [23]
WO_3-ZnO@rGO	Ultrasound	MB	0.0278 min^{-1}	94	90 [50]
TiO_2-ZnO	Hydrothermal	RhB	0.011 min^{-1}	89	180 [51]
ZnO-CdO-CuO	Co-precipitation	MB	0.027 min^{-1}	94	100 [52]
ZnO-Au-Cu_2O	Electrodeposition and sputtering	MO	0.3495 h^{-1}	~75	240 [24]
ZnO-WO_3	Sol–gel	MO	0.0521 min^{-1}	100	90 [53]
ZnO-Fe_3O_4-g-C_3N_4	Sol–gel and annellation	MO	0.0243 min^{-1}	~97	140 [54]
Ag-Cu_2O-ZnO NW	Hydrothermal and plasma–liquid	MO	0.165 min^{-1}	98	30 This work

Moreover, one of the critical factors for a good photocatalyst regarding large-scale production is stability. We, hence, conducted a repeated 20-cycle photocatalytic experiment to evaluate this factor under solar simulator illumination. The results are depicted in Figure 5f. After 10 cycles, the Ag-Cu_2O-ZnO photocatalyst still maintained great activity with a performance of ~97%. Although the catalytic activity continues to decrease in subsequent experimental cycles, the MO dye still decomposed to 95% in the 20th cycle, while that of the ZnO NWs significantly reduced by ~15% after 20 cycles. This result demonstrates the high stability of Ag-Cu_2O-ZnO in the visible light region. As expected, the synergistic contribution of the Ag/Cu_2O NPs improved the reusability of the Ag-Cu_2O-ZnO heterostructure. This demonstrates the superiority of a ternary structure in addressing chemical dyes that contaminate water sources.

In this work, the bottom of the conduction band (CB) and the top of the valence band (VB) of ZnO and Cu_2O are situated at −1.06 (V vs. NHE), 1.7 (V vs. NHE) and −0.77 (V vs. NHE), 2.57 (V vs. NHE), respectively [48]. Combined with the aforementioned findings and discussion, we propose a photocatalytic mechanism in the ternary Ag-Cu_2O-ZnO heterostructure, as illustrated in Figure 6.

The photocatalytic enhancement of this structure can be explained as follows: (i) The expansion of the absorption band to the visible light region due to the LSPR effect of Ag NPs and the narrow bandgap of Cu_2O (2.76 eV [53]) improves the light-harvesting efficiency. (ii) When exposed to visible light, the electrons from the Fermi level with the appearance of an LSPR effect are excited to a higher energy state; these electrons are thus moved to the CB of the Cu_2O. In the photocatalytic process, this can help raise the concentration of charge carriers, which is crucial for separating photogenerated electron–hole pairs [53]. (iii) Because of the p-n heterojunction and tight surface contact between ZnO and Cu_2O, photogenerated electrons continue to flow readily from the CB of Cu_2O to the CB of ZnO. As a result, the electrons on the CB of ZnO and the holes on the VB of Cu_2O can be split and

accumulated. The strong oxidants $\bullet O^{2-}$ and •OH, which take part in the MO degrading process, can be produced as a result of the redox process by the excess electrons on the CB of ZnO and holes on the VB of Cu_2O.

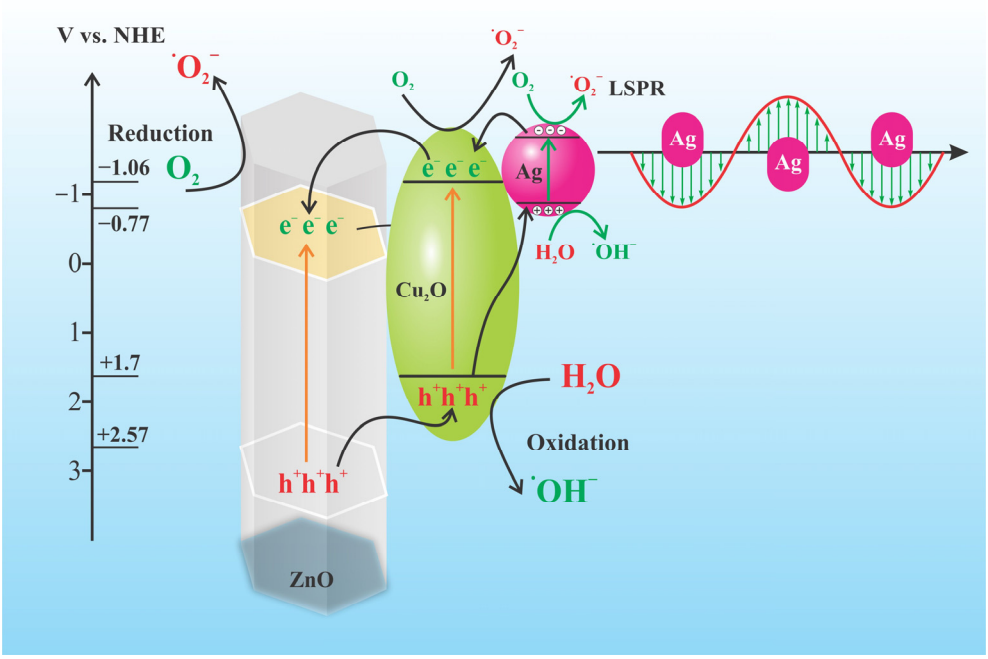

Figure 6. Proposed photocatalytic mechanism scheme of Ag−Cu_2O−ZnO ternary heterostructure.

3. Materials and Methods

Reagents: All chemicals used are analytic grade and high purity. $Zn(NO_3)_2$, Na_2CO_3, $AgNO_3$, $Cu(NO_3)_2$, NH_3, and L'-ascorbic acid were purchased from Sigma Aldrich (St. Louis, MO, USA), and deionized water was the solvent used to dissolve the applied chemicals. Distilled water and ethanol were utilized for cleaning.

3.1. Synthesis of ZnO Nanowires

ZnO nanowires (NWs) were prepared using the hydrothermal method with conditions outlined in our previous publication [28]. $Zn(NO_3)_2$ (0.05 M) and Na_2CO_3 (0.12 M) were separately dissolved in distilled water in two 100mL beakers for 1 h at room temperature. Prior to transferring the solutions to a Teflon put-in steel autoclave, these two solutions were mixed by a magnetic stirrer until the solution mixture reached a milky white color. The hydrothermal process was run at 200 °C for a full day. Eventually, after being taken out by a centrifuge, the white powder was repeatedly cleaned with distilled water and ethanol to get rid of the unreacted substances and contaminants. The powder was dried at 70 °C before being stored securely.

3.2. Decoration of Silver and Copper(I) Oxide on ZnO NWs Using the Plasma–Liquid Interaction Technique

Preparation of two precursor solutions:

(1) $AgNO_3$ salt was dissolved with deionized water in a 500 mL beaker in order to obtain a 50 mM Ag-precursor solution.

(2) We prepared a 15 mM L'ascorbic acid solution and a 50 mM $Cu(NO_3)_2$ solution in deionized water. In total, 50 mM of $Cu(NO_3)_2$ and 15 mM of L'ascorbic acid were combined in a 6:2 volumetric ratio to generate a Cu-precursor solution.

Setting up the plasma–liquid system:

A simple plasma–liquid system operating at ambient conditions comprises three main components, a DC high-voltage source, a plasma nozzle, and a gold electrode, described

in detail in Refs. [34,35]. The plasma nozzle, consisting of a plasma electrode comprising a 1.6 mm diameter Tungsten rod, was connected to an Ar gas flow system that was supplied during the experiment. The gold electrode was immersed in the examined solution contained in a 50 mL beaker. The DC power source supplied a high voltage of 2.5 kV to ignite the Ar gas plasma between the plasma nozzle and the aqueous solution surface. The generated current was kept at a constant value of 5 mA. Reactions in the solution were accelerated extraordinarily quickly owing to radicals and activated chemical species generated by plasma–liquid interactions.

The following steps were used to decorate the surface of the ZnO NWs with Ag and Cu_2O nanoparticles:

- The as-prepared ZnO NW powder was uniformly dispersed in distilled water within a 50 mL beaker using ultrasonic equipment.
- Plasma was ignited for three minutes.
- To form the ternary structure of Ag-Cu_2O-ZnO NWs, 5 mL of Cu-precursor solution was added, followed by five minutes of plasma treatment. Next, 80 µL of 50 mM Ag-precursor solution was added, and the plasma ignition process was continued for an additional five minutes.
- The Ag-Cu_2O-ZnO powder was isolated using centrifugation. These samples were dried in a vacuum oven for 24 h at 50 °C and stored in sealed vessels.

3.3. Sample Characterization

The surface morphology of the as-prepared samples was observed using field-emission scanning electron microscopy (FESEM, Hitachi S-4800, Tokyo, Japan). The crystal structure, composition, and morphology of the samples were certified by a high-resolution transmission electron microscope (HRTEM; JEM 2100, JEOL, Tokyo, Japan). Their crystal structure was determined by a Bruker D8 advanced X-ray power diffractometer with Cu-ka radiation. The photoluminescence spectrum was measured using high-resolution photoluminescence spectroscopy (Horiba iHR550, Horiba, Osaka, Japan) with the excitation of a 355 nm Teem Photonic laser and then detected using a thermoelectrically cooled Si-CCD camera (Horiba Synapse). The UV–vis absorption spectrum was examined by a Carry 5000 UV–vis spectrophotometer (Agilent, Santa Clara, CA, USA).

3.4. Photocatalytic Activity Evaluation

The photocatalytic activity of the samples involving ZnO and Ag-Cu_2O-ZnO was evaluated using the photodegradation of methyl orange (MO) under solar-simulated light. In total, 25 mg of photocatalyst was mixed with 30 mL of MO (5 ppm) contained in a beaker (Schott Duran, Mainz, Germany). After that, this mixture is stirred for an hour in a dark environment to ensure that the photocatalyst surface achieves an adsorption–desorption equilibrium state. Subsequently, the incident light source was irradiated perpendicularly to the solution surface for 30 min. Three milliliters of the solution were aspirated and placed in a centrifuge tube at determined intervals. The concentration of MO, with respect to the illuminated time interval, was measured using the UV–vis spectrophotometer.

4. Conclusions

Capitalizing on the advantages and effectiveness of the plasma–liquid method, we successfully synthesized a ternary Ag-Cu_2O-ZnO catalyst and proposed an underlying formation mechanism for this material system. The results showed that the coexistence of Cu_2O and Ag NPs on ZnO NWs acts as a key intermediate species for promoting fast charge transfer and separation and impeding electron–hole recombination. Indeed, the ternary Ag-Cu_2O-ZnO composite showed superior photocatalytic activity. About 82% and 98% of the MO contents decomposed under visible light irradiation within 10 and 30 min. In addition, the catalytic performance still achieved above 95% after 20 reuse cycles, indicating the excellent stability and reusability of the Ag-Cu_2O-ZnO. The findings demonstrate the

outstanding photocatalytic efficiency of semiconductor- and noble metal-based structures, paving the way for significant potential applications in pollutant treatments.

Author Contributions: Conceptualization, N.T.H.L., P.T.T. and V.D.L.; methodology, N.T.H.L. and T.X.A.; validation, N.T.H.L., P.T.T., V.H.K. and D.K.T.; formal analysis, P.T.T., N.T.H.L., T.N.B., V.H.K. and N.H.D.; investigation, P.T.T., T.N.B., L.T.H.P., V.D.L. and D.H.T.; data curation, P.T.T., L.T.H.P., V.H.K., D.K.T. and T.N.B.; writing—original draft preparation, P.T.T., D.H.M., N.H.D. and N.T.H.L.; writing—review and editing, N.T.H.L.; visualization, supervision, N.T.H.L., V.D.L. and D.H.M.; project administration, N.T.H.L.; funding acquisition, N.T.H.L. All authors have read and agreed to the published version of the manuscript.

Funding: This work was financially supported by the Ministry of Science and Technology, Vietnam, with the grant code NDT. 70.e-ASIA/19.

Data Availability Statement: The data that support the plots within this paper are available from the corresponding authors upon reasonable request.

Conflicts of Interest: The authors declare no conflicts of interest.

References

1. Al-Nuaim, M.A.; Alwasiti, A.A.; Shnain, Z.Y. The photocatalytic process in the treatment of polluted water. *Chem. Pap.* **2023**, *77*, 677–701. [CrossRef] [PubMed]
2. Ren, G.; Han, H.; Wang, Y.; Liu, S.; Zhao, J.; Meng, X.; Li, Z. Recent advances of photocatalytic application in water treatment: A review. *Nanomaterials* **2021**, *11*, 1804. [CrossRef]
3. Ong, C.B.; Ng, L.Y.; Mohammad, A.W. A review of ZnO nanoparticles as solar photocatalysts: Synthesis, mechanisms and applications. *Renew. Sustain. Energy Rev.* **2018**, *81*, 536–551. [CrossRef]
4. Qi, K.; Cheng, B.; Yu, J.; Ho, W. Review on the improvement of the photocatalytic and antibacterial activities of ZnO. *J. Alloys Compd.* **2017**, *727*, 792–820. [CrossRef]
5. Su, Q.; Zuo, C.; Liu, M.; Tai, X. A review on Cu_2O-based composites in photocatalysis: Synthesis, modification and applications. *Molecules* **2023**, *28*, 5576. [CrossRef]
6. Kuo, C.H.; Huang, M.H. Morphologically controlled synthesis of Cu_2O nanocrystals and their properties. *Nano Today* **2010**, *5*, 106–116. [CrossRef]
7. Consonni, V.; Briscoe, J.; Kärber, E.; Li, X.; Cossuet, T. ZnO nanowires for solar cells: A comprehensive review. *Nanotechnology* **2019**, *30*, 362001. [CrossRef]
8. Kandjani, A.E.; Sabri, Y.M.; Periasamy, S.R.; Zohora, N.; Amin, M.H.; Nafady, A.; Bhargava, S.K. Controlling core/shell formation of nanocubic p-Cu_2O/n-ZnO Toward Enhanced Photocatalytic Performance. *Langmuir* **2015**, *31*, 10922–10930. [CrossRef]
9. Chen, X.; Lin, P.; Yan, X.; Bai, Z.; Yuan, H.; Shen, Y.; Liu, Y.; Zhang, G.; Zhang, Z.; Zhang, Y. Three-dimensional ordered ZnO/Cu_2O nanoheterojunctions for efficient metal–oxide solar cells. *ACS Appl. Mater. Interfaces* **2015**, *7*, 3216–3223. [CrossRef]
10. Yoon, J.S.; Lee, J.W.; Sung, Y.M. Enhanced photoelectrochemical properties of Zscheme ZnO/p-n Cu_2O PV-PEC cells. *J. Alloys Compd.* **2019**, *771*, 869–876. [CrossRef]
11. Jiang, T.; Xie, T.; Chen, L.; Fu, Z.; Wang, D. Carrier concentration-dependent electron transfer in Cu_2O/ZnO nanorod arrays and their photocatalytic performance. *Nanoscale* **2013**, *5*, 2938–2944. [CrossRef]
12. Zou, X.; Tian, H.; Yan, S. Syntheis of Cu_2O/ZnO hetero-nanorod arrays with enhanced visible light-driven photocatalytic activity. *Cryst. Eng. Comm* **2014**, *16*, 1149–1156. [CrossRef]
13. Wang, X.-S.; Zhang, Y.-D.; Wang, Q.-C.; Dong, B.; Wang, Y.-J.; Feng, W. Photocatalytic activity of Cu_2O/ZnO nanocomposite for the decomposition of methyl orange under visible light irreadiation. *Sci. Eng. Compos. Mater.* **2019**, *26*, 104–113. [CrossRef]
14. Zhu, X.; Wang, J.; Yang, D.; Liu, J.; He, L.; Tang, M.; Feng, W.; Wu, X. Fabrication, characterization and high photocatalytic activity of Ag–ZnO heterojunctions under UV-visible light. *RSC Adv.* **2021**, *11*, 27257–27266. [CrossRef] [PubMed]
15. Deng, Q.; Duan, X.; Ng, D.H.L.; Tang, H.; Yang, Y.; Kong, M.; Wu, Z.; Cai, W.; Wang, G. Ag nanoparticle decorated nanoporous ZnO microrods and their enhanced photocatalytic activities. *ACS Appl. Mater. Interfaces* **2012**, *4*, 6030–6037. [CrossRef] [PubMed]
16. Trang, T.N.Q.; Phan, T.B.; Nam, N.D.; Thu, V.T.H. In situ charge transfer at the Ag@ZnO photoelectrochemical interface toward the high photocatalytic performance of H_2 evolution and RhB degradation. *ACS Appl. Mater. Interfaces* **2020**, *12*, 12195–12206. [CrossRef] [PubMed]
17. Thinh, V.D.; Lam, V.D.; Bach, T.N.; Van, N.D.; Manh, D.H.; Tung, D.H.; Lien, N.T.H.; Thuy, U.T.D.; Anh, T.X.; Tung, N.T.; et al. Enhanced optical and photocatalytic properties of Au/Ag nanoparticle-decorated ZnO films. *J. Electron. Mater.* **2020**, *49*, 2626–2632. [CrossRef]
18. He, W.; Kim, H.-K.; Wamer, W.G.; Melka, D.; Callahan, J.H.; Yin, J.-J. Photogenerated charge carrier and reactive oxygen species in ZnO/Au hybrid nanostructures with enhanced photocatalytic and antibacterial activity. *J. Am. Chem. Soc.* **2014**, *136*, 750–757. [CrossRef] [PubMed]

19. Mauro, A.D.; Zimbone, M.; Scuderi, M.; Nicotra, G.; Fragalà, M.E.; Impellizzeri, G. Effect of Pt nanoparticles on the photocatalytic activity of ZnO nanofibers. *Nanoscale Res. Lett.* **2015**, *10*, 484. [CrossRef]
20. Zhao, S.; Cheng, Z.; Kang, L.; Li, M.; Gao, Z. The facile preparation of Ag decorated TiO_2/ZnO nanotube and their potent photocatalytic degradation efficiency. *RSC Adv.* **2017**, *7*, 50064–50071. [CrossRef]
21. Mulkhopadhyay, S.; Maiti, D.; Chatterjee, S.; Devi, P.S.; Kumar, G.S. Design and application of Au decorated ZnO/TiO_2 as a stable photocatalyst for wide spectral coverage. *Phys. Chem. Chem. Phys.* **2016**, *18*, 31622–31633. [CrossRef]
22. Yin, H.; Yu, K.; Song, C.; Huang, R.; Zhu, Z. Synthesis of Au-decorated V_2O_5@ZnO heteronanostructures and enhanced plasmonic photocatalytic activity. *ACS Appl. Mater. Interfaces* **2014**, *6*, 14851–14860. [CrossRef]
23. Tsai, C.-E.; Yeh, S.-M.; Chen, C.-H.; Lin, H.-N. Flexible photocatalytic paper with Cu_2O and Ag nanoparticle-decorated ZnO nanorods for visible light photodegradation of organic dye. *Nanoscale Res. Lett.* **2019**, *14*, 204. [CrossRef] [PubMed]
24. Ren, A.; Wang, B.; Zhang, H.; Ding, P.; Wang, Q. Sandwiched ZnO@Au@Cu_2O Nanorod Films as Efficient Visible-Light-Driven Plasmonic Photocatalysts. *ACS Appl. Mater. Interfaces* **2015**, *7*, 4066–4074. [CrossRef] [PubMed]
25. Subash, B.; Krishnakumar, B.; Swaminathan, M.; Shanthi, M. ZnS–Ag–ZnO as an excellent UV-light-active photocatalyst for the degradation of AV 7, AB 1, RR 120, and RY 84 dyes: Synthesis, characterization, and catalytic applications. *Ind. Eng. Chem. Res.* **2014**, *53*, 12953–12963. [CrossRef]
26. Gavade, N.L.; Babar, S.B.; Kadam, A.N.; Gophane, A.; Garadka, K.M. Fabrication of M@CuxO/ZnO (M = Ag, Au) heterostructured nanocomposite with enhanced photocatalytic performance under sunlight. *Ind. Eng. Chem. Res.* **2017**, *56*, 14489–14501. [CrossRef]
27. Yuan, X.; Pei, F.; Luo, X.; Hu, H.; Qian, H.; Wen, P.; Miao, K.; Wang, W.; Feng, G. Fabrication of ZnO/Au@Cu2O heterojunction towards deeply oxidative photodegradation of organic dyes. *Sep. Purif. Technol.* **2021**, *262*, 118301. [CrossRef]
28. Thu, P.T.; Thinh, V.D.; Lam, V.D.; Bach, T.N.; Phong, L.T.H.; Tung, D.H.; Manh, D.H.; Van Khien, N.; Anh, T.X.; Le, N.T.H. Decorating of Ag and CuO on ZnO nanowires by plasma electrolyte oxidation method for enhanced photocatalytic efficiency. *Catalysts* **2022**, *12*, 801. [CrossRef]
29. Prete, P.; Lovergine, N.; Tapfer, L. Nanostructure size evolution during Au-catalysed growth by carbo-thermal evaporation of well-aligned ZnO nanowires on (100)Si. *Appl. Phys. A* **2007**, *88*, 21–26. [CrossRef]
30. Yatsui, T.; Lim, J.; Nakamata, T.; Kitamura, K.; Ohtsu, M.; Yi, G.-C. Low-temperature (∼270 °C) growth of vertically aligned ZnO nanorods using photoinduced metal organic vapour phase epitaxy. *Nanotechnology* **2007**, *18*, 065606. [CrossRef]
31. Liang, H.W.; Lu, Y.M.; Shen, D.Z.; Li, B.H.; Zhang, Z.Z.; Shan, C.X.; Zhang, J.Y.; Fan, X.W.; Du, G.T. Growth of vertically aligned single crystal ZnO nanotubes by plasma-molecular beam epitaxy. *Solid State Commun.* **2006**, *137*, 182–186. [CrossRef]
32. Fufa, P.A.; Feysia, G.B.; Gultom, N.S.; Kuo, D.-H.; Chen, X.; Kabtamu, D.M.; Zelekew, O.A. Visible light-driven photocatalytic activity of Cu2O/ZnO/Kaolinite-based composite catalyst for the degradation of organic pollutant. *Nanotechnology* **2022**, *33*, 315601. [CrossRef] [PubMed]
33. Shubha, J.P.; Adil, S.F.; Khan, M.; Hatshan, M.R.; Khan, A. Facile fabrication of a ZnO/Eu2O3/NiO-based ternary heterostruc-ture nanophotocatalyst and its application for the degradation of methylene Blue. *ACS Omega* **2021**, *6*, 3866–3874. [CrossRef] [PubMed]
34. Lee, S.Y.; Do, H.T.; Kim, J.H. Microplasma-assisted synthesis of TiO2–Au hybrid nanoparticles and their photocatalytic mechanism for degradation of methylene blue dye under ultraviolet and visible light irradiation. *Appl. Surf. Sci.* **2022**, *573*, 151383. [CrossRef]
35. Thuy, N.T.T.; Tung, D.H.; Manh, L.H.; Kim, J.H.; Kudryashov, S.I.; Minh, P.H.; Hien, N.T. Plasma enhanced wet chemical sur-face sctivation of TiO_2 for the synthesis of high-performance photocatalytic Au/TiO_2 nanocomposites. *Appl. Sci.* **2020**, *10*, 3345. [CrossRef]
36. Fatemeh, R.; Patrick, V.; Anton, N.; Rino, M.; Nathalie, D.G. Applications of plasma-liquid systems: A review. *Materials* **2019**, *12*, 2751.
37. Qiang, C.; Junshuai, L.; Yongfeng, L. A review of plasma–liquid interactions for nanomaterial synthesis. *J. Phys. D Appl. Phys.* **2015**, *48*, 424005.
38. Hu, H.; Huang, X.; Deng, C.; Chen, X.; Qian, Y. Hydrothermal synthesis of ZnO nanowires and nanobelts on a large scale. *Mater. Chem. Phys.* **2007**, *106*, 58–62. [CrossRef]
39. Yu, F.; Wang, C.; Li, Y.; Ma, H.; Wang, R.; Liu, Y.; Suzuki, N.; Terashima, C.; Ohtani, B.; Ochiai, T.; et al. Enhanced solar photothermal catalysis over solution plasma activated TiO_2. *Adv. Sci.* **2020**, *7*, 2000204. [CrossRef]
40. Qiang, C.; Toshiro, K.; Rikizo, H. Reductants in Gold Nanoparticle Synthesis Using Gas–Liquid Interfacial Discharge Plasmas. *Appl. Phys. Express* **2012**, *5*, 086201.
41. Li, Y.; Wang, Y.; Lin, J.; Shi, Y.; Zhu, K.; Xing, Y.; Li, X.; Jia, Y.; Zhang, X. Solution-plasma-induced oxygen vacancy enhances MoO_x/Pt electrocatalytic counter electrode for bifacial dye-sensitizes solar cells. *Front. Energy Res.* **2022**, *10*, 924515. [CrossRef]
42. Pitchaimuthu, S.; Honda, K.; Suzuki Shoki Naito, A.; Suzuki, N.; Katsumata, K.; Nakata, K.; Ishida, N.; Kitamura, N.; Idemoto, Y.; Kondo, T.; et al. Solution plasma process-derived defect-induced heterophase anatase/brookite TiO_2 nanocrystals for enhanced gaseous photocatalytic performance. *ACS Omega* **2018**, *3*, 898–905. [CrossRef]
43. Kondeti, V.S.; Gangal, U.; Yatom, S.; Bruggeman, P.J. Ag^+ reduction and silver nanoparticle at the plasma-liquid interface by an RF driven atmospheric pressure plasma jet: Mechanisms and the effect of surfactant. *J. Vac. Sci. Technol. A Vac. Surf. Film.* **2017**, *35*, 061302. [CrossRef]
44. Leonardo, V.; Ignacio, C.; Javier, E.; Nancy, B.; Dinesh, P.S. Ascorbic acid based controlled growth of various Cu and Cu_2O nanostructures. *Mater. Res. Express* **2019**, *6*, 065033.

45. Mariotti, D.; Patel, J.; Švrček, V.; Maguire, P. Plasma-liquid interactions at atmospheric pressure for nanomaterials synthesis and surface engineering. *Plasma Process. Polym.* **2012**, *9*, 1074–1085. [CrossRef]
46. Zheng, K.; Zhang, Z.; Wang, X.; Zhan, R.; Chen, H.; Deng, S.; Xu, N.; Chen, J. Mechanism of photoluminescence quenching in visible and ultraviolet emissions of ZnO nanowires decorated with gold nanoparticles. *Jpn. J. Appl. Phys.* **2019**, *58*, 051005. [CrossRef]
47. Wu, H.-Y.; Jian, W.-J.; Dang, H.-F.; Zhao, X.-F.; Zhang, L.-Z.; Li, J.-H. Hierarchical Ag-ZnO Microspheres with Enhanced Photocatalytic Degradation Activities. *Pol. J. Environ. Stud.* **2017**, *26*, 871–880. [CrossRef]
48. Cui, J.; Ye, L.; Chen Xi Li, J.; Bian Yang Yang, M.; Yang, Q.; Yun, D.; Sun, S. Simultaneously promoting adsorption and charge separation in Z-scheme ZnO/Cu_2O heterojunctions for efficient removal of tetracycline. *Appl. Surf. Sci.* **2023**, *638*, 158046. [CrossRef]
49. Reynolds, D.C.; Look, D.C.; Jogai, B.; Litton, C.W.; Cantwell, G.; Harsch, W.C. Valence-band ordering in ZnO. *Phys. Rev. B* **1999**, *60*, 2340–2344. [CrossRef]
50. Chaudhary, K.; Shaheen, N.; Zulfiqar, S.; Sarwar, M.I.; Suleman, M.; Agboola, P.O.; Shakir, I.; Warsi, M.F. Binary WO_3-ZnO nanostructures supported rGO ternary nanocomposite for visible light driven photocatalytic degradation of methylene blue. *Synth. Met.* **2020**, *269*, 116526. [CrossRef]
51. Tran Thi, V.H.; Pham, T.N.; Pham, T.T.; Le, M.C. Synergistic Adsorption and Photocatalytic Activity under Visible Irradiation Using Ag-ZnO/GO Nanoparticles Derived at Low Temperature. *J. Chem.* **2019**, *2019*, 2979517. [CrossRef]
52. Munawar, T.; Yasmeen, S.; Hussain, F.; Mahmood, K.; Hussain, A.; Asghar, M.; Iqbal, F. Synthesis of novel heterostructured ZnO-CdO-CuO nanocomposite: Characterization and enhanced sunlight driven photocatalytic activity. *Mater. Chem. Phys.* **2020**, *29*, 122983. [CrossRef]
53. Ashiegbu, D.C.; Potgieter, H.J. ZnO-based heterojunction catalysts for the photocatalytic degradation of methyl orange dye. *Heliyon* **2023**, *9*, e20674. [CrossRef] [PubMed]
54. Wu, Z.; Chen, X.; Liu, X.; Yang, X.; Yang, Y. A Ternary Magnetic Recyclable ZnO/Fe_3O_4/g-C_3N_4 Composite Photocatalyst for Efficient Photodegradation of Monoazo Dye. *Nanoscale Res. Lett.* **2019**, *14*, 147. [CrossRef]